Digital Filters for Reducing Background Noise in Micro PIV Measurements

by

L. Gui[1], S. T. Wereley[2] and S.Y. Lee[3]

Mechanical Engineering, Purdue University West Lafayette, IN 47907-1288

E-Mail: [1]guil@purdue.edu, [2]wereley@purdue.edu, and [3]leesy1@purdue.edu

ABSTRACT

In the present work digital filters are used to reduce the measurement uncertainty of the microscopic particle image velocimetry (μPIV) technique. Analysis shows that single pixel random noise and low frequency background noise in the μPIV recordings are much stronger than in the usual macroscopic PIV recordings. The effects of several different low- and high-pass filters on the evaluation accuracy of a correlation-based interrogation algorithm with continuous window shift and central difference image correction are investigated. Simulations show that the 3×3-pixel rectangular smooth filter can reduce effectively the evaluation error resulting from single pixel random noise. The unsharp mask is a powerful tool to reduce the evaluation error caused by low frequency background noise. A μPIV image filter that combines the capabilities of both the smooth filter and the unsharp mask is constructed to enable high accuracy evaluation of μPIV recordings.

The μPIV image filter is applied in the PIV experiment of water flow in a deep microchannel of 200μm×600μm×120mm. As shown in in Fig.1, the μPIV recordings have a strong singe pixel random noise level and low frequency noises of different wavelengths. Averaged correlation functions are given in Fig.2a and 2b, respectively, for the cases with and without using μPIV image filter. Fig.2a shows that in the case without filtering the low frequency noise results in a dominant peak in the evaluation function at zero displacement. The correlation peak of the particle image displacement can not be identified in the presence of this noise peak. When the μPIV image filter is used to remove the low frequency noise, a clear peak of the particle image displacement is observed, see Fig.2b. The axial velocity (U) profile of the fully developed microchannel flow is shown in Fig.3a. The distributions of the standard deviation (σ) of the axial velocity are provided in Fig.3b. The test results show that a much lower precision error level can be achieved by using μPIV image filter.

Abbreviations

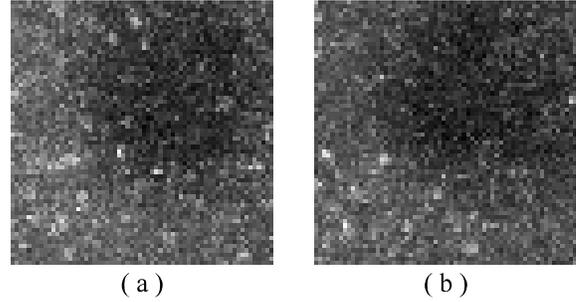|	
CCWS	correlation-based interrogation algorithm with continuous window shift
CDIC	central difference image correction
FFT	fast Fourier transformation
μPIV	micro particle image velocimetry
PIV	particle image velocimetry
RMS	root-mean-square
RSS	root-sum-square

(a)   (b)

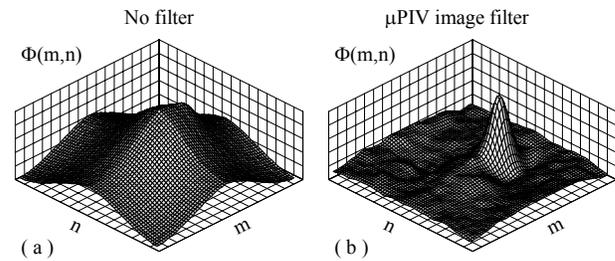**Fig. 1**: μPIV evaluation sample pair (64×64 pixels)

Fig. 2: Correlation funcns: (a) No filter, (b) Using μPIV image filter.

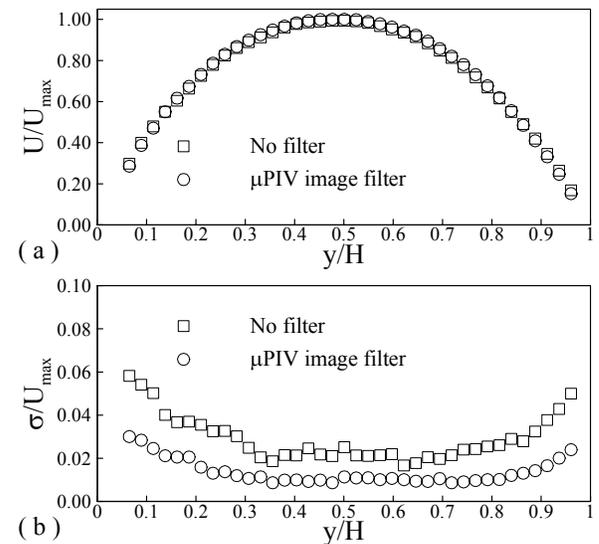**Fig. 3:** Velocity profile (a) measured using μPIV in a microchannel and the standard deviation (b) of the measurement results

1. INTRODUCTION

Micro particle image velocimetry is becoming a general tool for investigating flows in micro-scale devices. Santiago, et al. (1998) described the first μPIV system consisting of an epi-fluorescent microscope, an intensified CCD camera and a continuous Hg-arc lamp capable of measuring slow flows in micro devices with a spatial resolution of $6.9 \times 6.9 \times 1.5$ μm^3. μPIV was used to measure slow flows around a red blood cell with a spatial resolution of 3.5×3.5 μm^2 (Wereley et al. 1998). Later applications of the μPIV technique moved steadily toward faster flows by replacing the continuous Hg-arc lamp with a two-headed Nd:YAG laser and an interline transfer camera, with which singly-exposed PIV recording pairs can be acquired with a sub-microsecond time interval (Meinhart et al., 1999; Meinhart and Zhang, 2000). Wereley et al. (2002) reviewed μPIV details and recent advances in the technique. Currently, volume illumination, small particles and Brownian motion are three fundamental problems that differentiate μPIV from conventional macroscopic PIV. The first two of these problems reduce the contrast between μPIV particle images and the background to levels significantly lower than that for macroscopic PIV. Generally, the image quality of μPIV recordings is much lower than that of macroscopic PIV recordings, and the μPIV recordings usually have a low image density.

The correlation-based interrogation and tracking algorithms are usually used to evaluate the μPIV recordings. The correlation-based interrogation algorithm has played a major role in evaluating PIV recordings since the first application of the digital PIV technique. It correlates the gray value distributions in two equal-sized interrogation windows, one chosen from each of the two digital images comprising a PIV recording pair. The correlation computation is usually accelerated with the fast Fourier transformation (FFT) algorithm. Details of the correlation-based interrogation algorithm were described, discussed, and reviewed by Cenedese and Paglialunga (1990), Keane and Adrian (1990), Adrian (1991), Willert and Gharib (1991), Heckmann et al. (1994), and Westerweel et al. (1996). Using the FFT algorithm brings several problems to the correlation-based interrogation algorithm, such as large evaluation errors at large particle image displacements and large bias gradient around zero displacement, which increase the measurement uncertainties of the mean velocities and Reynolds stresses, respectively, in turbulent flow measurements (Gui et al. 2001). In order to avoid the large evaluation errors at large particle image displacements, a discrete window shift is often applied (Willert 1996; Westerweel et al. 1997). For reducing the bias error and bias gradient around the zero displacement, a Gaussian window mask is adopted (Gui et al. 2000, 2001). The correlation function has also been used as a tracking criterion for determining the displacement of an image pattern that contains a group of particle images. Correlation-based tracking schemes were described and applied by Huang et al. (1993), Kemmerich and Rath (1994), Okamoto et al. (1995), and Fincham and Spedding (1997). When using a correlation-based tracking algorithm, the first interrogation window defines the particle image pattern to be tracked, while the second interrogation window determines the tracking area, so that the second interrogation window is larger than the first. In comparison with the original correlation-based interrogation, the correlation-based tracking achieves a higher accuracy at large particle image displacements and avoids the large bias error and bias gradient around zero displacement, so that it was considered to be a better algorithm for a long time period. However, a multi-pass continuous window shift technique largely increases the evaluation accuracy of the correlation-based interrogation scheme (Sjödahl, 1994; Sholl et al., 1997; Lecordier et al., 1999, 2001). An evaluation conducted by Gui and Wereley (2002) indicated that when combined with the continuous window shift technique the correlation-based interrogation algorithm exhibits much better performance than the correlation-based tracking algorithm. Further advances of the evaluation algorithm are the central difference interrogation (Wereley et al., 1998; Wereley and Meinhart, 2000, 2001) and particle image pattern correction (Huang et al., 1993; Tokumaru and Dimotakis, 1995; Fincham and Spedding, 1997; Lin and Perlin, 1998; Nogueira et al, 1999, 2001; Scarano, 2002). Recently, Wereley and Gui (2001, 2002) described a central difference image correction (CDIC) method that combines ideas of central difference interrogation, adaptive continuous window shift and particle image pattern correction, enabling a very reliable and accurate evaluation of digital PIV recordings in a wide variety of circumstances. In order to increase the signal-to-noise ratio of the μPIV recordings, Meinhart, et al. (2000) developed an average correlation method that is widely used in the evaluation of μPIV recordings.

Digital filters are basic tools for improving the quality of digital images. They are described in many books related to digital signal and image processing, e.g. Lim (1990). In general, low-pass filters can be used to reduce the high frequency noise sources in digital images, whereas high-pass filters can be used to minimize the low-frequency noise. Many researchers tried to apply the digital filters to increase the measurement accuracy of PIV, e.g. Mass (1992), Heckmann (1996) and Gui (1998). However, improper use of digital filters in PIV recording evaluation may cause serious problems. For instance, the high-pass filter may strengthen random noise sources and low-pass filters may eliminate the fine structures of particle images. In the present work, the effects of several different digital filters on the evaluation accuracy of μPIV recordings by using the correlation-based interrogation with continuous window shift and image correction are investigated. A new digital filter is constructed to enable a high accuracy evaluation of μPIV recordings and applied in PIV tests conducted in a microchannel.

2. PIV IMAGE AND BACKGROUND NOISE

When the tracer particles illuminated by the laser are small enough to be considered as point light sources, they have an intensity distribution given by the Airy function, which is reasonably well approximated by a Gaussian function. The Gaussian distribution of a particle image intensity (gray value) in the image plane (x,y) can be described by

$$G_P(x,y) = G_c \exp\left(-2\frac{(x-x_0)^2 + (y-y_0)^2}{D_p{}^2}\right) \qquad (1)$$

where D_P, G_c and (x_0,y_0) are diameter, center brightness and position of the particle image, respectively. The traditional macroscopic PIV technique usually requires the particle image diameter to be around 1.5 pixels to achieve the maximal accuracy of the correlation-based interrogation algorithm. However, particle images in μPIV recordings are usually much larger, i.e. D_P=3~6 pixels. Usually, the Airy or Gaussian distributions of particle images can hardly be identified in μPIV recordings because of strong background noise sources.

Fig. 4: Histogram of a micro-PIV recording

The most frequently observed noise in μPIV recordings results from thermal noise in the CCD array. Since this noise is related to individual pixels and has a random intensity distribution, we refer it to as single pixel random noise. The single pixel random noise (G_{sp}) includes a constant portion G_0 and a random portion G_r, i.e.

$$G_{sp}(x,y) = G_o + G_r(x,y) \qquad (2)$$

G_r has a Gaussian probability distribution in the μPIV recording and can be quantified with the root-mean-square (RMS) value

$$G_{rms} = \sqrt{\frac{1}{MN}\sum_{x=1}^{M}\sum_{y=1}^{N}G_r^2(x,y)} \qquad (3)$$

where M and N are width and height of the digital PIV recording, respectively. In the following we refer G_{rms} to the intensity of single pixel random noise. As an example, the probability distribution function of gray value in a digital PIV recording taken in a micro channel is given in Fig. 4 in form of a histogram. An image sample of 32×32 pixels is also shown in this figure. The histogram has a Gaussian peak centered at 41 that indicates the mean gray value of the background. The standard deviation of the gray values around the mean ($\approx G_{rms}$) is 8. The gray level of the particles in this μPIV recording is around 150.

Another kind of background noise results from non-uniform illumination, particle clusters out of the focal plane, unexpected reflection etc. It has a relatively low spatial frequency, and in many cases, it is unchanged from frame to frame. In order to investigate its influence on the evaluation accuracy of the μPIV recordings, the following function is used to simulate the low frequency background noise:

$$G_{lf}(x,y) = A_{lf}\sin\left(\frac{2\pi \cdot x}{\lambda_x}+\phi\right)\cdot\sin\left(\frac{2\pi \cdot y}{\lambda_y}+\varphi\right) \qquad (4)$$

Wherein A_{lf} is the amplitude of the low frequency background noise; λ_x and λ_y are the wavelength in x- and y-direction, respectively; ϕ and φ are the initial phases.
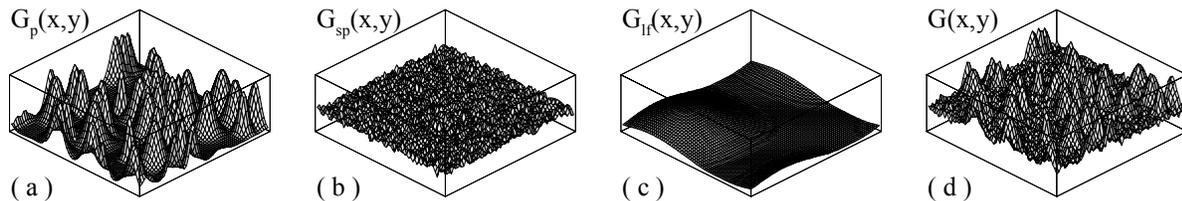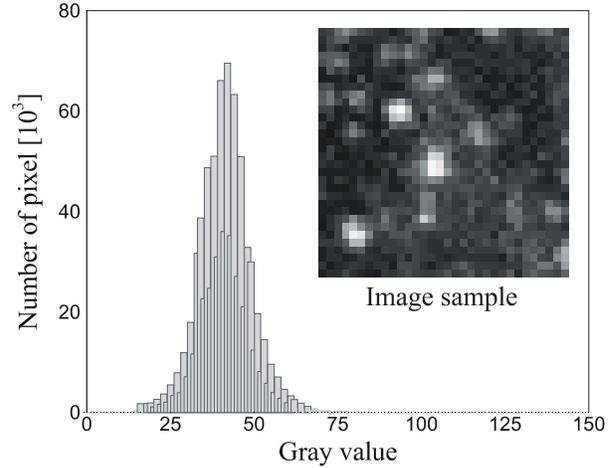

(a) (b) (c) (d)

Fig. 5: Components of intensity distribution in μPIV recording

As illuminated in Fig.5, the total gray value distribution of the μPIV recording (G) is considered as a root-sum-square (RSS) of the Gaussian particle images (G_p), the single pixel random noise (G_{sp}), and the low frequency background noise (G_{lf}), i.e.

$$G(x,y) = \sqrt{G_P^2(x,y) + G_{sp}^2(x,y) + G_{lf}^2(x,y)} \tag{5}$$

Most of following discussions are based on synthetically generated PIV recording pairs of size of 1024×1024 pixels. The total particle number N_{tot} is given to determine the particle image number density. The particle position (x_0, y_0) are determined by a random number generator with uniform probability distribution in the image plane. The particle image brightness and diameter, G_c and D_p are also randomly determined in some of the simulations by a similar procedure. G_0 is given to determine the mean value of the single pixel random noise. $G_r(x,y)$ has a Gaussion probability distribution that is determined by a given G_{rms}. The low frequency background noise is generated with equation (4). A four-roll-mill flow (Wereley and Gui 2001) is simulated by synthetic PIV recording pairs with zero displacement in the center and 0.52 pixels at the four corners, so that the particle image displacements evaluated with a 16×16-pixel grid structure have an uniform distribution between –0.5 and 0.5 pixels.

3. μPIV IMAGE FILTERING
3.1. Digital filters
The simplest kind of digital filter is the linear homogeneous filter defined by

$$G'(x,y) = \sum_{-r}^{r} \sum_{-r}^{r} C(i,j) \cdot G(x-i, y-j) \tag{6}$$

where $C(i,j)$ is the coefficient of the filter mask of size of $(2r+1) \times (2r+1)$; G and G' are the gray value distribution of the digital image before and after filtering, respectively. With different filter masks, different low- and high-pass filters are constructed in the linear homogeneous filter family. The simplest low-pass filter is the rectangular smooth filter determined by filter mask

$$C(i,j) = \frac{1}{(2r+1) \cdot (2r+1)} \quad \text{for } -r \le i \le r \text{ and } -r \le j \le r. \tag{7}$$

Examples of simple high-pass filters are

$$\text{Gradient filter: } C = \frac{1}{2} \begin{bmatrix} 0 & -1 & 0 \\ -1 & 2 & 0 \\ 0 & 0 & 0 \end{bmatrix}, \tag{8}$$

$$\text{Laplace filter: } C = \frac{1}{4} \begin{bmatrix} 0 & -1 & 0 \\ -1 & 4 & -1 \\ 0 & -1 & 0 \end{bmatrix}. \tag{9}$$

The gradient filter is one of several filters that conduct the first order differential operation. The Laplace filter conducts the second order differential operation. A more complicated high-pass filter, i.e. the unsharp mask, has been applied to digital PIV recordings by some researchers to remove the low frequency background noise. It is defined as

$$G'(x,y) = G(x,y) - \frac{1}{(2r+1) \cdot (2r+1)} \sum_{-r}^{r} \sum_{-r}^{r} G(x-i, y-j) \tag{10}$$

The size of the unsharp mask should be determined according to the spatial frequencies of particle images and noises.

3.2. Effects of digital filters on PIV recording evaluation
Our investigation begins with tests of the 3×3-pixel smooth filter, gradient filter and Laplace filter using synthetic PIV recording pairs with ideal Gaussian particle images, i.e. without any noise. 14 synthetic PIV recording pairs are generated with total particle number N_{tot}=20480, brightness G_c=250 and particle image diameters D_P=0.5~6 pixels. These synthetic PIV recording pairs are processed with the three different digital filters, respectively, and then evaluated using the CCWS method. A 16×16-pixel evaluation grid structure and a 32×32-pixel interrogation window are used in the evaluation. The RMS evaluation errors for different particle image diameters and different digital filters are given in Fig. 6. The test results show that the gradient filter and Laplace filter can only reduce the evaluation error when the particle image diameter is larger than 5 pixels, otherwise they increase the evaluation error. The 3×3-pixel smooth filter effectively

reduces the evaluation error at small particle diameters but increases the evaluation error at large particle diameters. The minimal evaluation errors in the cases with and without the smooth filter are almost the same, and it seems that the smooth filter shifts the minimal point of the evaluation error distribution from 3 pixels to 1.5 pixels.

The smooth filter is further tested with synthetic PIV recording pairs that include the single pixel random noise. 8 pairs of synthetic PIV recordings are generated with different noise intensities. In these synthetic PIV recording pairs the parameters are set as N_{tot}=10240, G_0=90, G_c=180, and D_P=3~6 pixels (i.e. particle image size range of most current μPIV recordings). These synthetic PIV recording pairs are processed with the rectangular smooth filter of four different mask sizes respectively and then evaluated using CCWS with a 32×32-pixel interrogation window. The evaluation error dependence on the noise intensity is shown in Fig. 7. The evaluation errors without filtering are also given in the figure for comparison. The test results indicate that the 3×3-pixel smooth filter effectively reduces the evaluation error at high noise intensity, (G_{rms}/G_c>0.1), and it just slightly increases the evaluation error at low random noise intensity. The smooth filters of larger mask size generally increase the evaluation error, except for the 5×5-pixel smooth filter in the region of G_{rms}/G_c>0.15. Additional investigations show that the influence of the mean noise value G_0 on the evaluation uncertainty is very small in comparison with that of the random noise intensity G_{rms}.

The effects of high-pass filters are investigated using synthetic PIV recording pairs with low frequency background noise. The particle image parameters are set as N_{tot}=20480, G_0=90, G_c=180, and D_P=3~6 pixels. The simulated low frequency background noise has a wavelength of 512 pixels, and its amplitude varies in the region of A_{lf}/G_c=0~1. The investigation is conducted with two steps: in the first step there is no single pixel random
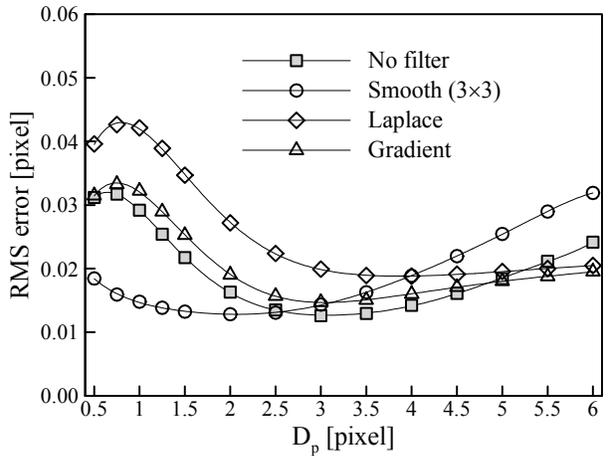

Fig.6: Evaluation error of for ideal particle images processed with different filters
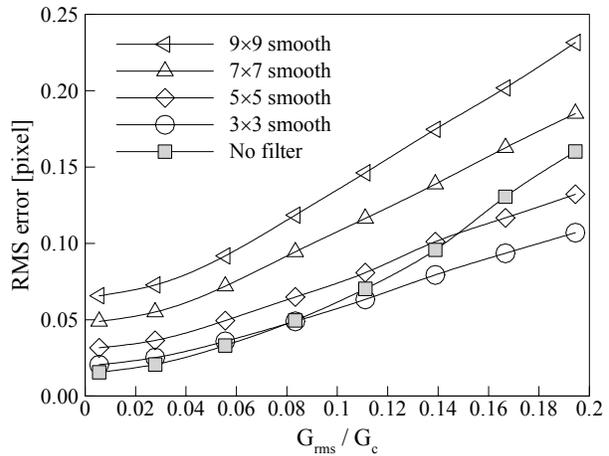
Fig. 7: Evaluation error distributions on the random noise intensity for different smooth filters

noise, whereas in the second step single pixel random noise of G_{rms}/G_c=0.056 is added. These synthetic PIV recording pairs are processed with the gradient filter, Laplace filter and 21×21-pixel (r=10) unsharp mask, respectively, and then evaluated using the CCWS algorithm with a 64×64-pixel interrogation window. The test results are given in Fig. 8, in
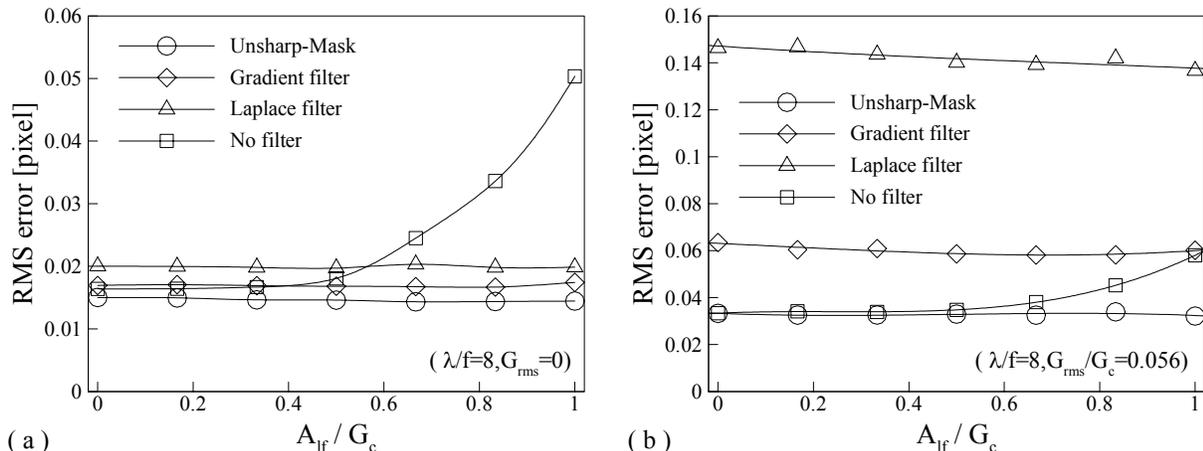

(a)

(b)

Fig. 8: Test results of three different high-pass filters using synthetic PIV recording pairs with low frequency noise: (a) No random noise, (b) With random noise

which symbol f (=64) represents the side length of the interrogation window. Test results in Fig.8a show that the evaluation error without filtering increases rapidly when the relative amplitude of the low frequency noise increases at A_{lf}/G_c>0.5. When the high-pass filters are applied, the evaluation errors do not depend on the amplitude of the low frequency noise; i.e. the high-pass filters completely remove the influence of the low frequency noise. Fig.8b shows that the evaluation errors of the gradient filter and Laplace filter become very large when the single pixel random noise is added. The 21×21-pixel unsharp mask has very good performance in both test cases, i.e. with and without random noises. The influence of the unsharp mask filter size on the evaluation accuracy is further investigated with two pairs of synthetic PIV recordings. One of them does not have any noise, whereas another has the single pixel random noise of G_{rms}/G_c=0.056. The particle image parameters are set as N_{tot}=10240, G_0=90, G_c=180, and D_P=3~6 pixels. The two

Fig. 9: Evaluation error distributions on the filter side length of the unsharp mask

synthetic PIV recording pairs are processed with the unsharp mask of different side lengths and then evaluated using the CCWS algorithm with a 32×32-pixel interrogation window. The test results, including those without filtering, are given in Fig.9. Fig.9 shows that the unsharp mask of small filter size (e.g. <9 pixels) may increase the evaluation error like the gradient filter and Laplace filter, but it has no side effects when the filter side length is not less than twice of the maximal particle image diameter, i.e. ≥12 pixels in this test case.
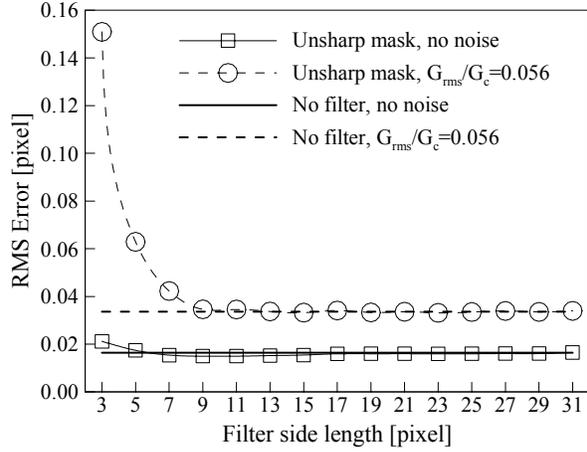
3.3. µPIV image filter

According to investigations in section 3.2, the 3×3-pixel rectangular smooth filter can be used effectively to remove the single pixel random noise, whereas the unsharp mask is an ideal tool to remove the low frequency background noise. To simplify the filter operation and reduce potential rounding errors, a new digital filter that combines features of the two previous filters is constructed as

$$G'(x,y) = \frac{1}{9}\sum_{-1}^{1}\sum_{-1}^{1}G(x-i,y-j) - \frac{1}{(2r+1)(2r+1)}\sum_{-r}^{r}\sum_{-r}^{r}G(x-i,y-j). \qquad (11)$$

When using Eq.(6), the filter coefficient is determined by

$$C(i,j) = \begin{cases} \dfrac{1}{9} - \dfrac{1}{(2r+1)\cdot(2r+1)} & \text{If } -1 \le i \le 1 \text{ and } -1 \le j \le 1 \\[4mm] -\dfrac{1}{(2r+1)\cdot(2r+1)} & \text{otherwise} \end{cases} \qquad (12)$$

The new filter is named the µPIV image filter, because it is designed to remove the strong single pixel random noise and low frequency noise from µPIV recordings. As indicated in Fig.9, the radius of the µPIV image filter (r) should be larger than the maximal particle image diameter.

4. APPLICATION EXAMPLE

The µPIV image filter is applied in the PIV experiment of water flow in a deep microchannel, which has a rectangular cross-section of 200×600 µm^2 and a length of 120mm. The fluorescent polystyrene particles (Duke Scientific, Palo Alto, CA) used for the present experiment have a peak excitation wavelength of 542 nm and 612 nm for emission. The diameter and density of the particles are 0.69µm and 1050 kg/m^3, respectively. The pulsed laser beam is generated by a double cavity NewWave Nd:YAG laser, delivered into the inverted epi-fluorescent microscope (Nikon TE200) through the beam expander assembly, and guided to the flow field of the microchannel through a set of lenses inside the microscope and finally through a 20X microscope objective lens. The fluorescent particles suspended in the flow field absorb the illuminating light of λ=532nm (green) and emit light with a longer wavelength (λ~612nm, red), which passes through the fluorescent filter cube into a Lavision Flowmaster 3S CCD camera of digital resolution of 1024×1280 pixels. The corresponding measurement area in the focal plane is 348.3×435.4 µm^2. Measurements are conducted at different positions along the channel with Reynolds number varying from hundreds to thousands to investigate transitions from laminar to turbulent flow in micro scale as well as the effect length scale and boundary conditions on entrance length.

The time interval between laser pulses is carefully set so that the particle image displacements are around 10 pixels. 100 PIV recording pairs are taken for each case to enable use of the average correlation algorithm. A test is conducted downstream of the channel far from the entrance ($67D_h$) at Re=1707. As shown in an evaluation sample pair in Fig.1, the μPIV recordings have a strong singe pixel random noise level ($G_{rms}/G_c{\approx}0.12$), and low frequency noises of different wavelengths can be observed easily, e.g. the dark spot in Fig.1 that probably results from some debris depositing on the glass cover of the microchannel. The averaged correlation function of 100 evaluation sample pairs at the same location as the pair of images shown in Fig.1 are given in Fig.2a and 2b, respectively, for the cases with and without using μPIV image filter. Fig.2a shows that in the case without filtering the low frequency noise results in a dominant peak in the evaluation function at zero displacement. The correlation peak of the particle image displacement can not be identified in the presence of this noise peak. When the μPIV image filter is used to remove the low frequency noise, a clear peak of the particle image displacement is observed , see Fig.2b.

In order to quantify the effects of the μPIV image filter on the evaluation of real μPIV recordings, the μPIV recording pairs are evaluated by using CDIC and average correlation method with and without μPIV image filter, respectively. The axial velocity (U) profile of the fully developed microchannel flow is determined by averaging data at 160 cross-section cuts and shown in Fig.3a. The distributions of the standard deviation (σ) of the axial velocity are provided in Fig.3b. The test results show that a much lower precision error level can be achieved by using μPIV image filter. Note that the velocity is normalized with the maximum velocity (U_{max}) and the coordinate with the channel width (H).

5. SUMMARY AND CONCLUSIONS

The present work is aimed to reducing the measurement uncertainty of μPIV by using digital filters to remove background noise in digital PIV recordings. The performance of the rectangular smooth filter, gradient filter, Laplace filter and unsharp mask are tested with synthetically generated PIV recording pairs. Simulations show that the 3×3-pixel gradient and Laplace filter are very sensitive to the single pixel random noise, so that they are suggested not to be used in processing μPIV recordings. The 3×3-pixel rectangular smooth filter can be used effectively to remove the single pixel random noise, but larger smooth filter sizes are not suggested. When the filter size is large enough, the unsharp mask can be used to minimize the low frequency background noise without any noticeable side effects. A μPIV image filter that combines the capabilities of both the 3×3-pixel smooth filter and the unsharp mask is constructed to enable high accuracy evaluation of μPIV recordings in a single processing step. This new μPIV digital filter was applied to a microchannel flow, demonstrating the performance of the new digital filter and confirming the simulation results. Although the analyses presented here are based on the correlation-based interrogation algorithms with continuous window shift, the conclusions can be extended to other processing techniques.

REFERENCES
Adrian RJ (1991), Particle-Imaging Techniques for Experimental Fluid Mechanics. Annu. Rev. Fluid Mech. 23, 261-304

Cenedese A; Paglialungga A (1990), Digital direct analysis of a multiexposed photograph in PIV. Exp. Fluids 8,

Fincham AM; Spedding GR (1997), Low cost, high resolution DPIV for measurement of turbulent fluid flow. Exp. Fluids 23, 449-462

Gui L (1998) Methodische Untersuchungen zur Auswertung von Aufnahmen der digitalen Particle Image Velocemetry. Shaker Verlag, Aachen, Germany

Gui L; Merzkirch W; Fei R (2000) A digital mask technique for reducing the bias error of the correlation-based PIV interrogation algorithm, Exp. Fluids 29: 30-35

Gui L;. Longo J; Stern F (2001), Biases of PIV measurement of turbulent flow and the masked correlation-based interrogation algorithm. Exp. Fluids 30, pp. 27-35

Gui L; Wereley ST (2002) A correlation-based continuous widow shift technique for reducing the peak locking effect in digital PIV image evaluation. Exp. Fluids 32: 506-517

Heckmann W; Hilgers S; Merzkirch W; Schlüter T (1994), Automatic Evaluation of Double-Exposed PIV Records by an Autocorrelation Method. Optical Methods and Data Processing in Heat and Fluid Flow, C485/021, City University, London,UK

Heckmann W (1996) Auswertealgorithmen in der Particle Image Velocimetry. Shaker Verlag, Aachen, Germany

Huang HT; Fiedler HE; Wang JJ (1993), Limitation and improvement of PIV — Part I: Limitation of conventional techniques due to deformation of particle image patterns. Exp. Fluids 15, 168-174

Huang HT; Fiedler HE; Wang JJ (1993), Limitation and improvement of PIV — Part II: Particle image distortion, a novel technique. Exp. Fluids 15, 263-273

Keane RD; Adrian RJ (1990), Optimization of particle image velocimeters. Part I: Double pulsed systems, Meas. Sci. Technol. 1, 1202-1215

Kemmerich Th; Rath HJ (1994), Multi-level convolution filtering technique for digital laser-speckle-velocimetry. Exp. Fluids 17, 315-322

Lecordier B; Lecordier JC; Trinité M (1999), Iterative sub-pixel algorithm for the cross-correlation PIV measurements. 3rd Int. Workshop on PIV, September 16-19, Santa Barbara

Lecordier B; Demare D; Vervish LMJ; Réveillon J; Trinité M (2001), Estimation of the accuracy of PIV treatment for turbulent flow studies by direct numerical simulation of milti-phase flow. Meas. Science and Technology 12: 1382-1391

Lim JS (1990) Two dimensional signal and image processing. PRENTICE HALL, Englewood Cliffs, New Jersey 07632

Maas HG (1992), Digitale Photogrammetrie in der dreidimensionalen Strömungsmeßtechnik, Diss. ETH Nr. 9665

Meinhart CD, Wereley ST, Santiago JG (1999) PIV measurements of a microchannel flow, Exp. Fluids, Vol. 27, 414-419

Meinhart CD, Wereley ST, Santiago JG (2000) A PIV algorithm for estimating time-averaged velocity fields, Journal of Fluids Engineering, Vol. 122, 285-289

Meinhart CD and Zhang H (2000) The flow structure inside a microfabricated inkjet printer head, J. Microelectromechanical Systems, Vol. 9, 67-75

Okamoto K; Hassan YA; Schmidl WD (1995), New tracking algorithm for particle image velocimetry. Exp. Fluids 19, 342-347

Santiago JG, Wereley ST, Meinhart CD, Beebe DJ, Adrian RJ 1998, A particle image velocimetry system for microfluidics. Exp. Fluids 25, 316-319

Scarano F (2002) Iterative image deformation methods in PIV. Meas. Sci. Tech. 13 (1): R1-R19 JAN 2002

Sholl MJ; Savas Ö (1997), A fast Lagrangian PIV method for study of general high gradient flow. 35th AIAA Aerospace Science Meeting, Reno, NV, Jan 6-9, AIAA paper 97-0493 (A97-15543)

Sjödahl M (1994), Electronic speckle photography: increased accuracy by nonintegral pixel shift. Applied Optics 33(28): 6667-6673

Tokumaru PT; Dimotakis PT (1995) Image correlation velocimetry. Exp Fluids 19: 1-15

Wereley ST, Santiago JG, Meinhart CD, Adrian RJ 1998, Velocimetry for MEMS Applications. Proc. of ASME/DSC, Vol. 66, (Micro-fluidics Symposium, November, Anaheim, CA)

Wereley ST; Gui L; Meinhart CD (2002) Advanced algorithms for microscale velocimetry. AIAA Journal Vol. 40, #6

Wereley ST; Gui L (2001) PIV measurement in a four-roll-mill flow with a central difference image correction (CDIC) method, 4th International Symposium on Particle Image Velocimetry, Göttingen, Germany, Sept. 17-19

Wereley ST; Gui L (2002) A correlation-based central difference image correction (CDIC) method and application in a four-roll-mill flow PIV measurement. Exp. Fluids (submitted)

Westerweel J; Draad A; Hoeven J; Oord J (1996), Measurement of fully-developed turbulent pipe flow with digital particle image velocimetry, Exp. Fluids 20, 165-177

Westerweel J; Dabiri D; Gharib M (1997), The effect of a discrete window offset on the accuracy of cross-correlation analysis of digital PIV recordings, Exp. Fluids 23, 20-28

Willert CE (1996), The fully digital evaluation of photographic PIV recordings. Appl. Sci. Res. 56, 79-102

Willert CE; Gharib M (1991), Digital Particle Image Velocimetry. Exp. Fluids 10, 181-193